First-Principles Approach to Calculating Energy Level Alignment at Aqueous Semiconductor Interfaces

Neerav Kharche,[1,*] James T. Muckerman,[1,†] and Mark S. Hybertsen[2,‡]

[1]*Department of Chemistry, Brookhaven National Laboratory, Upton, New York 11973-5000, USA*
[2]*Center for Functional Nanomaterials, Brookhaven National Laboratory, Upton, New York 11973-5000, USA*

A first-principles approach is demonstrated for calculating the relationship between an aqueous semiconductor interface structure and energy level alignment. The physical interface structure is sampled using density functional theory based molecular dynamics, yielding the interface electrostatic dipole. The *GW* approach from many-body perturbation theory is used to place the electronic band edge energies of the semiconductor relative to the occupied $1b_1$ energy level in water. The application to the specific cases of nonpolar $(10\bar{1}0)$ facets of GaN and ZnO reveals a significant role for the structural motifs at the interface, including the degree of interface water dissociation and the dynamical fluctuations in the interface Zn-O and O-H bond orientations. These effects contribute up to 0.5 eV.

The alignment of electronic energy levels at a hetero-interface between two materials represents both a fundamental materials interface characteristic and a crucial property that controls electronic device functionality in such diverse areas as semiconductor electronics, batteries, and electrochemical cells. In the case of semiconductor interfaces, the energy level alignment is encapsulated in the valence band edge energy offset, and a hierarchy of theoretical approaches to calculate it have been established [1]. However, the corresponding energy level alignment at solid-electrolyte interfaces poses a substantially more complex problem. In particular, development of a constructive, first-principles theory for the alignment of semiconductor band-edge potentials to electrochemical potentials still presents fundamental challenges [2].

As a significant example, the relative alignment of the semiconductor band edge and the corresponding redox level in the solvent for a target reaction determines, thermodynamically, whether photoexcited carriers in the semiconductor can drive the reaction and with what range of overpotential. This is of fundamental importance in the design of electrochemical devices for solar energy harvesting [3,4]. In particular, it is an unavoidable constraint in the search for materials that can serve both as efficient absorbers of the solar spectrum and to supply electrons and holes with sufficient energy to drive relevant reactions, e.g., the hydrogen evolution reaction or the water oxidation reaction.

In practical electrochemical measurements, the interface presents a complex system: a doped semiconductor, an aqueous interface of generally unknown atomic structure that may well participate in acid-base reactions, and the water with dissolved ions and a particular *p*H. Through control of the applied bias and the *p*H, conditions corresponding to both flat bands in the semiconductor and zero zeta potential in the water can be achieved. The latter refers to the condition of zero net interface charge due to acid-base activity at the interface (adsorption of H^+ and OH^-) [2]. Under these conditions, the interface specific alignment of the semiconductor band edges to the scale of redox levels in water can be measured. In turn, this alignment determines semiconductor band bending and water double-layer formation under general conditions of doping, ion concentration, bias, and *p*H.

In order to circumvent the complexity of these interfaces and seek trends across semiconductors, a simplified picture is appealing [5]. Imagine opening up the interface so that one can characterize a reference semiconductor surface and a water surface separately [Fig. 1(a)]. On the water side, the positions of the highest occupied states of bulk water ($1b_1$) are known from photoemission measurements [6]. The $H^+/(1/2)H_2$ redox level defines the standard hydrogen electrode (SHE) and its absolute value relative to vacuum has been established [2,7]. On the semiconductor side, the ionization potential and electron affinity fix the band edge positions relative to the vacuum. Taken together, a model of the energy level alignment emerges. What additional physical effects at the real interface alter this simple picture and how large are they?

In order to probe the impact of realistic semiconductor-water interface structure, a constructive theory for the energy level alignment is required. While distinct approaches have been explored [2,8–10], at a key point in the analysis, Kohn-Sham energy eigenvalues from density functional theory (DFT) are used to approximate electronic excitation energies. This is well known to fail formally and practically, e.g., the well-known band gap problem [11]. The *GW* approach, in many-body perturbation theory, offers a well-founded theory for excitation energies [12–14]. Recent applications of the *GW* approach
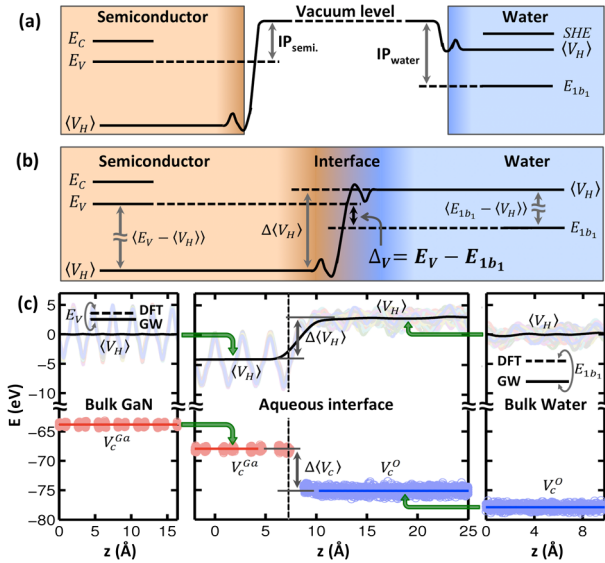
FIG. 1 (color online). (a) Simplified model for energy level alignment based on separate semiconductor and water energies with respect to vacuum. (b) Schematic for energy level alignment including the potential step due to the physical interface structure. Valence band energy level offset Δ_V breaks into three contributions in Eq. (1) and shown here. (c) Illustration of the separate calculation of each of those three terms for the specific case of energy level alignment at the GaN($10\bar{1}0$)-water interface. Center panel: Results of the full interface simulation. Top: Planar, running, and time (thermal) average of the electrostatic potential ($\langle V_H \rangle$, black line) superposed over 50 individual, planar-averaged snapshots. Bottom: Time and space averaged core potentials superposed over individual values from the same snapshots. Left panel: Bulk GaN simulation showing E_V for GaN from DFT and GW superposed on the averaged electrostatic potential and the averaged core potentials. Right panel: Bulk water showing E_{1b_1} superposed on the same averaged potentials. Final energy level alignment requires shifting left and right panels in energy relative to the center panel as illustrated by the arrows to get the final alignment as in (b). Either V_H or, equivalently, the core potentials can be used for alignment.

to liquid water demonstrate substantial corrections for key electronic levels [15,16]. For trends in electrochemical energy level alignment, based on the simplified model in Fig. 1(a), recent studies have incorporated corrections from the GW approach [17–19]. The broadest survey considered the calculated band edges, the available photoemission data for the semiconductor surfaces, and electrochemical data [19]. The authors infer that semiconductor-water interface structure contributes about 0.5 eV to the alignment, albeit without explicit treatment of such structure.

Here, we demonstrate a first-principles approach to calculating the electronic excitation energy level alignment at specific semiconductor-water interfaces [$\Delta_V = E_V - E_{1b_1}$, Fig. 1(b)]. To do so, we must integrate dynamical sampling of the physical and electronic structure of both water and the aqueous interface with the GW approach for the excitation energies.

Our approach builds on the established methodology used for semiconductor interfaces [1,20–23]. DFT is utilized for the microscopic charge distribution at the interface, responsible for the interface-specific intrinsic dipole, while the GW approach is used for the calculation of the excitation energies in the semiconductor and in the water. Three separate calculations are required: one each for the bulk materials and a third for the interface properties. The final energy level alignment combines the results from these three calculations as illustrated in Fig. 1(c), where the suitably averaged electrostatic potential (V_H) or core potential is used for reference.

To represent the properties of the solid-liquid interface, *ab initio* molecular dynamics (MD) are used to simulate ambient conditions. Electronic properties are determined by averaging a sample of configurations to represent the thermal average and include the impact of finite temperature renormalization of the energy levels, albeit in a semiclassical approximation [24,25]. Our theory provides the semiconductor valence band alignment to the centroid of the $1b_1$ band in liquid water

$$\Delta_V = E_V - E_{1b_1} = \langle E_V^{GW} - \langle V_H \rangle \rangle_{T,\text{bulk}}$$
$$- \langle E_{1b_1}^{GW} - \langle V_H \rangle \rangle_{T,\text{bulk}} + \Delta \langle \langle V_H \rangle_{\text{planar}} \rangle_{T,\text{interface}}. \quad (1)$$

This result links to the electrochemical scales in water and the vacuum scale through the E_{1b_1}.

We demonstrate our approach for the specific cases of GaN and ZnO ($10\bar{1}0$) interfaces with water, motivated by the utility of GaN/ZnO mixed crystals for photocatalysis
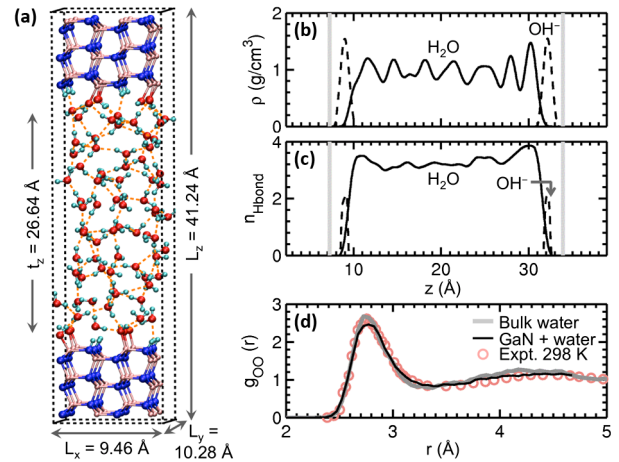

FIG. 2 (color online). GaN-water interface simulation. (a) Snapshot from the equilibrated portion of the MD simulation illustrating the unit cell. (b) Planar and time averaged density of water molecules (black solid line) and OH^- ions (black dashed line) as a function of distance between the GaN interfaces (vertical gray lines). (c) Average number of hydrogen bonds for water molecules (solid black line) and OH^- ions (black dashed line) (d) Calculated O-O pair distribution function from the bulk water simulation (gray line) and the GaN interface simulation (black line) together with experiment [26].

with visible light [27] and the recent observation that the
$(10\bar{1}0)$ facet dominates the activity for GaN nanowires [28].
We have recently analyzed the atomic-scale structure at
these aqueous semiconductor interfaces using DFT-based
MD simulations, demonstrating the role of interface water
dissociation [29]. The same technical protocol is used here
[30–36], including use of the projector augmented wave
(PAW) method [30] as implemented in VASP [31,32], with
the functional optB88-vdW [34,35] that includes long-
range van der Waals interactions. See the Supplemental
Material for details [37].

A snapshot of the equilibrated structure for the GaN case
[Fig. 2(a)] shows that water near the interface with GaN
spontaneously dissociates resulting in a fully hydroxylated
surface, in agreement with prior work [29,38,39]. All
surface N sites are protonated while all surface Ga sites
are bonded to the corresponding OH$^-$ ions. The average
density of water, the characteristics of the hydrogen bonds,
the valence band density of states (DOS, not shown), and
the O-O pair distribution function (excluding the near-
surface regions) are close to those calculated for bulk water
[Figs. 2(b)–2(d)] and experiment [26]. For the ZnO inter-
face, the interface water layer is partially dissociated. Half
of the adsorbed water molecules dissociate for a 4×2
interface cell, in agreement with earlier studies [29,40,41].
For a 3×2 cell, in-plane boundary conditions result in
fluctuations in the fraction of water dissociated at the
interface, including intervals where it is 67%, providing
another structure for study.

To extract the average potential step between the semi-
conducting region and the water region, the electrostatic
potential profile is calculated for 50 snapshots sampled
from a 5 ps window. These are averaged laterally to obtain
the traces shown in Fig. 1(c), followed by a running average
and a time average. The resulting average electrostatic
potential is flat both in the center of the semiconducting
region and in the center of the water region; interface effects
are localized. In practice, the PAW core potential, illus-
trated in Fig. 1(c), provides an accurate, physically equiv-
alent approach. It is readily available for every MD
snapshot and averages are performed using all snapshots
in the chosen time window. Comparison of averages over a
series of shorter time windows (1–2 ps each), suggests an
error bar of less than 0.1 eV due to sampling [37].

For the electronic excitation energies, the *GW* calcu-
lations are done with a full-frequency, spectrum-only self-
consistent approach, as implemented in VASP [42,43].
These specific choices in the method are based on previous
results for the energy band alignment at the Si-SiO$_2$
interface where this level of *GW* self-consistency gave
calculated band offsets within 0.3 eV of measured values
[23]. Convergence with respect to the number of empty
states is achieved by a hyperbolic fit to a series of
calculations and extrapolation [37,44]. For the case of
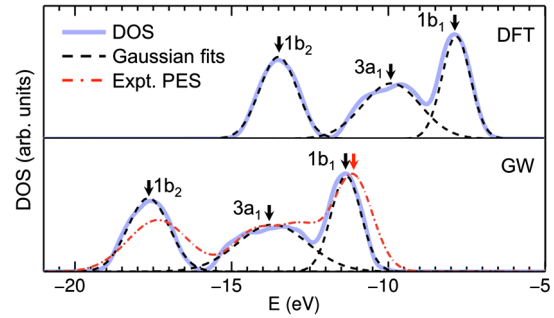water, electronic states of the 32 molecule cell are analyzed

FIG. 3 (color online).   Valence band density of states (DOS) of
bulk water, relative to the vacuum level, calculated using DFT
(top) and *GW* (bottom). Experimental PES spectra [6] shown
(bottom) with intensity scaled to match theory near the $1b_1$ peak.

for a sample of 50 snapshots over a 5 ps period, using *GW*
for a subset of 12 snapshots with the same energy gap
distribution.

With this level of the theory, as expected [43], the
calculated bulk band gaps of GaN (4.00 eV) and ZnO
(3.93 eV) are somewhat too large in comparison to
experiment (3.44 and 3.3 eV, respectively) [45,46], all at
room temperature [37]. Also, the optimized GaN and ZnO
lattice constants are about 1% smaller than the experimental
values [37], which contributes a 0.2–0.3 eV increase to the
band gap through the deformation potentials [45]. For bulk
water, the calculated average band gap based on DFT is
4.35 eV while the present *GW* approach gives 9.53 eV,
slightly larger than the experimental value of 8.7 ± 0.5 eV
[47]. Our use of spectrum-only self-consistency accounts
for the increase relative to the recent G_0W_0 result (8.1 eV
[16]). Furthermore, the binding energies of the occupied
$3a_1$ band and $1b_2$ band relative to the $1b_1$ band (see Fig. 3)
are much more accurate in the present *GW* calculations
(2.34 and 6.30 eV) than for the DFT energies (2.05 and
5.66 eV) in comparison to photoemission experiments
(2.34 and 6.21 eV) [6].

Next, we analyze the ingredients for the simple picture of
Fig. 1(a). From the MD simulation of a water slab [37], we
find $\Delta\langle V_H \rangle = -3.32$ eV at the water-vacuum interface, in
good agreement with earlier studies [16,48–50]. Using this
value, the calculated bulk DOS for water is aligned relative
to the vacuum level and compared with the experimental
PES [6] in Fig. 3. The binding energies are underestimated
in DFT while the *GW* corrected binding energies are in
very good agreement with the experimental data, particu-
larly the $1b_1$ level (peak centroid) at -11.32 eV, compared
to the measured value of -11.16 eV [6]. For the clean GaN
and ZnO $(10\bar{1}0)$ surfaces, including relaxation, the valence
band edge with respect to vacuum is calculated to be -6.98
and -8.08 eV, respectively. We make a direct comparison
to photoemission experiments for the closely related
ZnO$(11\bar{2}0)$ surface, for which we calculated -8.14 eV,
in good agreement, for an absolute energy, with the
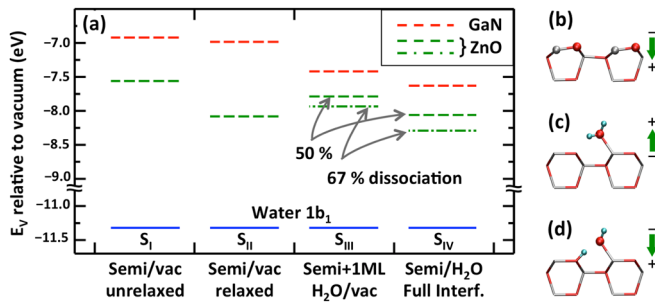measured value, -7.82 eV [51]. See Ref. [19] for a broader

FIG. 4 (color online). (a) Valence band edges, relative to vacuum, of GaN and ZnO for different surface and interface configurations ($S_I - S_{IV}$). Solid horizontal lines depict the $1b_1$ level of water relative to vacuum. For the full interface case, S_{IV}, it is used with the calculated offset Δ_V to place the semiconductor valence band relative to vacuum. Atomistic schematics with the qualitative induced surface dipole shown (green arrows) due to: (b) relaxation of the clean ZnO surface, (c) molecular, and (d) dissociative water adsorption, both on the ideal ZnO surface.

survey. From these calibration examples for both ZnO and water, the highest occupied level is slightly too deep relative to vacuum, an error that partially cancels in the final theoretical results for the band alignment below. Overall, this suggests that errors in the band alignment at the aqueous interface will be similar to those found previously for the Si-SiO$_2$ interface with the same level of GW self-consistency [23].

The alignment of E_V to the $1b_1$ level in water according to the simplified scheme is shown in Fig. 4(a) (S_{II}). The results for the ideal, unrelaxed semiconductor surfaces are also shown (S_I). Relaxation leads to rotation of the surface bond with outward (inward) displacement of the anion (cation) and an induced dipole at the surface pointing inwards [Fig. 4(b)] which lowers E_V relative to vacuum. This is a much larger effect for ZnO due to its more ionic bond.

Next, we show the results from the full calculation, including the structure of the semiconductor-water interface [Fig. 1(b)]. The calculated offsets ($\Delta_V = E_V - E_{1b_1}$) are placed on the vacuum scale using the calculated value for the $1b_1$ level from the water slab calculation [Fig. 4(a), S_{IV}]. For GaN, the change from the simple model is substantial, with E_V shifting to -7.63 eV. For ZnO, the degree of interface water dissociation is quantitatively important, with the final placement of E_V being -8.06 and -8.29 eV for 50% and 67% dissociation, respectively. In contrast to the GaN case, the simple model for ZnO is surprisingly close to the overall result from the full calculation. Analysis of the induced surface dipoles shows opposing effects from the molecular and dissociative adsorption of water [Figs. 4(c) and 4(d)]. For GaN, lifting the surface reconstruction is dominated by dissociative adsorption of water which lowers E_V. For ZnO, the effect of lifting the reconstruction is larger while the mixture of molecular and dissociative water adsorption compete, with the latter being more significant in the 67% dissociative case.

To obtain more insight into the role of interface structure motifs, we show results in Fig. 4(a) (S_{III}) for each semiconductor with a single monolayer of adsorbed water in vacuum, with the degree of dissociation found at the full interface. The structures are fully relaxed, representative of a surface experiment. The result for GaN, -7.42 eV, is rather close to the full calculation. This suggests that the additional dipole induced by interaction of the hydroxylated surface with liquid water is minimal. On the other hand, the results for the ZnO case (-7.79 and -7.94 eV) agrees somewhat less well with the full calculations. Interestingly, key interface cation-O and O-H bond orientations fluctuate much more in the ZnO case compared to the GaN case. Correspondingly, the impact of the dipole contribution from the liquid water interface to the hydroxylated surface is also larger, another interface structure specific result. However, our results do suggest that a well-chosen, hydroxylated surface may be a better choice for application of the simple picture in Fig. 1(a) for semiconductors that actively promote water dissociation.

Electrochemical experiments for GaN [52,53] and for ZnO [54,55] show acid-base activity at the semiconductor-water interface, with a clear rise of the measured band edge positions with solution pH (from 47 to 55 meV per pH unit, close to the ideal, Nernstian case of 59 meV). Therefore, an additional measurement must determine the pH at which the interface is neutral, assuring the equivalent of flat-band conditions on the water side of the junction. This has not been measured for GaN, but it is in the range of pH = 8 to 10 for ZnO [56,57]. Taken together with the measured potential for the band edges [54,55], the data are tightly clustered and relatively independent of facet, covering a range of about 0.3 eV, centered on $E_V = -7.3$ eV relative to vacuum. With reference to Fig. 4(a), the value of E_V from experiment is at higher energy than that predicted here for the ZnO ($10\bar{1}0$) interface with a partially dissociated water layer. It is also above the value from the simple picture of Fig. 1(a), (experimental value, -7.82 eV). Considering the impact on the dipole of different species at the interface (Fig. 4), this suggests that under realistic electrochemical conditions, another structural element with an opposite dipole to the net effect seen here must be involved. Possibilities include alternative structures that result from the etching of the ZnO or the role of adsorption of other ions from solution, both factors discussed in early literature [54,56,58].

In summary, we demonstrate the integrated use of state-of-the-art techniques for the first-principles treatment of energy level alignment at aqueous semiconductor interfaces. The initial, calibrated applications to GaN ($10\bar{1}0$) and ZnO ($10\bar{1}0$), which exhibit different degrees of both water dissociation and cation-O and O-H bond fluctuations at the interface, demonstrate the significant role of interface structure and dynamics. In the future, this approach will support an improved microscopic understanding of chemical interactions and the impact of interface structure on the

fundamental energy alignments across semiconductor-water interfaces.

---

[*]nkharche@bnl.gov
[†]muckerma@bnl.gov
[‡]mhyberts@bnl.gov

[1] A. Franciosi and C. G. Van de Walle, Surf. Sci. Rep. **25**, 1 (1996).
[2] J. Cheng and M. Sprik, Phys. Chem. Chem. Phys. **14**, 11245 (2012).
[3] A. J. Nozik and R. Memming, J. Phys. Chem. **100**, 13061 (1996).
[4] A. Kudo and Y. Miseki, Chem. Soc. Rev. **38**, 253 (2009).
[5] M. A. Butler and D. S. Ginley, J. Electrochem. Soc. **125**, 228 (1978).
[6] B. Winter, R. Weber, W. Widdra, M. Dittmar, M. Faubel, and I. V. Hertel, J. Phys. Chem. A **108**, 2625 (2004).
[7] S. Trasatti, Pure Appl. Chem. **58**, 955 (1986).
[8] J. Cheng and M. Sprik, Phys. Rev. B **82**, 081406 (2010).
[9] Y. Wu, M. K. Y. Chan, and G. Ceder, Phys. Rev. B **83**, 235301 (2011).
[10] H. Cheng and A. Selloni, Langmuir **26**, 11518 (2010).
[11] R. O. Jones and O. Gunnarsson, Rev. Mod. Phys. **61**, 689 (1989).
[12] M. S. Hybertsen and S. G. Louie, Phys. Rev. B **34**, 5390 (1986).
[13] R. W. Godby, M. Schlüter, and L. J. Sham, Phys. Rev. B **35**, 4170 (1987).
[14] W. G. Aulbur, L. Jonsson, and J. W. Wilkins, in *Solid State Physics*, edited by H. Ehrenreich and F. Spaepen (Academic, New York, 2000), Vol. 54, pp. 1–218.
[15] C. W. Swartz and X. Wu, Phys. Rev. Lett. **111**, 087801 (2013).
[16] T. A. Pham, C. Zhang, E. Schwegler, and G. Galli, Phys. Rev. B **89**, 060202 (2014).
[17] M. C. Toroker, D. K. Kanan, N. Alidoust, L. Y. Isseroff, P. Liao, and E. A. Carter, Phys. Chem. Chem. Phys. **13**, 16644 (2011).
[18] Y. Li, L. E. O'Leary, N. S. Lewis, and G. Galli, J. Phys. Chem. C **117**, 5188 (2013).
[19] V. Stevanovic, S. Lany, D. S. Ginley, W. Tumas, and A. Zunger, Phys. Chem. Chem. Phys. **16**, 3706 (2014).
[20] C. G. Van de Walle and R. M. Martin, Phys. Rev. B **34**, 5621 (1986).
[21] S. B. Zhang, D. Tomanek, S. G. Louie, M. L. Cohen, and M. S. Hybertsen, Solid State Commun. **66**, 585 (1988).
[22] M. S. Hybertsen, Appl. Phys. Lett. **58**, 1759 (1991).
[23] R. Shaltaf, G. M. Rignanese, X. Gonze, F. Giustino, and A. Pasquarello, Phys. Rev. Lett. **100**, 186401 (2008).
[24] M. Lax, J. Chem. Phys. **20**, 1752 (1952).
[25] M. Cardona and M. L. W. Thewalt, Rev. Mod. Phys. **77**, 1173 (2005).
[26] A. K. Soper and C. J. Benmore, Phys. Rev. Lett. **101**, 065502 (2008).
[27] K. Maeda, K. Teramura, D. L. Lu, T. Takata, N. Saito, Y. Inoue, and K. Domen, Nature (London) **440**, 295 (2006).
[28] D. F. Wang, A. Pierre, M. G. Kibria, K. Cui, X. G. Han, K. H. Bevan, H. Guo, S. Paradis, A. R. Hakima, and Z. T. Mi, Nano Lett. **11**, 2353 (2011).
[29] N. Kharche, M. S. Hybertsen, and J. T. Muckerman, Phys. Chem. Chem. Phys. **16**, 12057 (2014).
[30] P. E. Blöchl, Phys. Rev. B **50**, 17953 (1994).
[31] G. Kresse and J. Furthmuller, Phys. Rev. B **54**, 11169 (1996).
[32] G. Kresse and D. Joubert, Phys. Rev. B **59**, 1758 (1999).
[33] L. L. Jensen, J. T. Muckerman, and M. D. Newton, J. Phys. Chem. C **112**, 3439 (2008).
[34] M. Dion, H. Rydberg, E. Schroder, D. C. Langreth, and B. I. Lundqvist, Phys. Rev. Lett. **92**, 246401 (2004).
[35] J. Klimes, D. R. Bowler, and A. Michaelides, Phys. Rev. B **83**, 195131 (2011).
[36] Springer Materials, Landolt-Bornstein Database, http://www.springermaterials.com/docs/index.html.
[37] See Supplemental Material at http://link.aps.org/supplemental/10.1103/PhysRevLett.113.176802, which includes plots that illustrate the core potential offsets as a function of time and the extrapolation of the *GW* calculations versus the number of empty states.
[38] X. A. Shen, Y. A. Small, J. Wang, P. B. Allen, M. V. Fernandez-Serra, M. S. Hybertsen, and J. T. Muckerman, J. Phys. Chem. C **114**, 13695 (2010).
[39] J. Wang, G. Roman-Perez, J. M. Soler, E. Artacho, and M. V. Fernandez-Serra, J. Chem. Phys. **134**, 024516 (2011).
[40] O. Dulub, B. Meyer, and U. Diebold, Phys. Rev. Lett. **95**, 136101 (2005).
[41] G. Tocci and A. Michaelides, J. Phys. Chem. Lett. **5**, 474 (2014).
[42] M. Shishkin and G. Kresse, Phys. Rev. B **74**, 035101 (2006).
[43] M. Shishkin and G. Kresse, Phys. Rev. B **75**, 235102 (2007).
[44] C. Friedrich, M. C. Muller, and S. Blugel, Phys. Rev. B **83**, 081101 (2011).
[45] I. Vurgaftman and J. R. Meyer, J. Appl. Phys. **94**, 3675 (2003).
[46] V. Srikant and D. R. Clarke, J. Appl. Phys. **83**, 5447 (1998).
[47] A. Bernas, C. Ferradini, and J. P. Jay-Gerin, Chem. Phys. **222**, 151 (1997).
[48] K. Leung, J. Phys. Chem. Lett. **1**, 496 (2010).
[49] S. M. Kathmann, I.-F. W. Kuo, C. J. Mundy, and G. K. Schenter, J. Phys. Chem. B **115**, 4369 (2011).
[50] M. Lucking, Y.-Y. Sun, D. West, and S. Zhang, Chem. Sci. **5**, 1216 (2014).
[51] R. K. Swank, Phys. Rev. **153**, 844 (1967).

[52] S. S. Kocha, M. W. Peterson, D. J. Arent, J. M. Redwing, M. A. Tischler, and J. A. Turner, J. Electrochem. Soc. **142,** L238 (1995).

[53] J. D. Beach, R. T. Collins, and J. A. Turner, J. Electrochem. Soc. **150,** A899 (2003).

[54] W. P. Gomes and F. Cardon, Prog. Surf. Sci. **12,** 155 (1982).

[55] Y. Matsumoto, T. Yoshikawa, and E. Sato, J. Electrochem. Soc. **136,** 1389 (1989).

[56] L. Blok and P. L. De Bruyn, J. Colloid Interface Sci. **32,** 518 (1970).

[57] C. Kunze, M. Valtiner, R. Michels, K. Huber, and G. Grundmeier, Phys. Chem. Chem. Phys. **13,** 12959 (2011).

[58] J. F. Dewald, J. Phys. Chem. Solids **14,** 155 (1960).